Geophys. J. Int. (1998) **133,** 379–389

A continuous plate-tectonic model using geophysical data to estimate plate-margin widths, with a seismicity-based example

Caroline Dumoulin,* David Bercovici† and Pål Wessel

Department of Geology & Geophysics, School of Ocean and Earth Science and Technology, University of Hawaii, Honolulu, HI 96822, *USA.*
E-mail: dberco@soest.hawaii.edu

Accepted 1997 November 7. Received 1997 November 6; in original form 1997 March 4

SUMMARY

A continuous kinematic model of present-day plate motions is developed which (1) provides more realistic models of plate shapes than employed in the original work of Bercovici & Wessel (1994), and (2) provides a means whereby geophysical data on intraplate deformation is used to estimate plate-margin widths for all plates. A given plate's shape function (which is unity within the plate and zero outside the plate) can be represented by analytic functions as long as the distance from a point inside the plate to the plate's boundary can be expressed as a single-valued function of azimuth (i.e. a single-valued polar function). To allow sufficient realism to the plate boundaries, without the excessive smoothing used by Bercovici & Wessel, the plates are divided along pseudo-boundaries; the boundaries of plate sections are then simple enough to be modelled as single-valued polar functions. Moreover, the pseudo-boundaries have little or no effect on the final results. The plate shape function for each plate also includes a plate-margin function which can be constrained by geophysical data on intraplate deformation. We demonstrate how this margin function can be determined by using, as an example data set, the global seismicity distribution for shallow (depths less than 29 km) earthquakes of magnitude greater than 4. Robust estimation techniques are used to determine the width of seismicity distributions along plate boundaries; these widths are then turned into plate-margin functions, that is analytic functions of the azimuthal polar coordinate (the same azimuth of which the distance to the plate boundary is a single-valued function). The model is used to investigate the effects of 'realistic' finite-margin widths on the Earth's present-day vorticity (i.e. strike-slip shear) and divergence fields as well as the kinetic energies of the toroidal (strike-slip and spin) and poloidal (divergent and convergent) flow fields. The divergence and vorticity fields are far more well defined than for the standard discontinuous plate model and distinctly show the influence of diffuse plate boundaries such as the northeast boundary of the Eurasian plate. The toroidal and poloidal kinetic energies of this model differ only slightly from those of the standard plate model; the differences, however, are systematic and indicate a greater proportion of spin kinetic energy in the continuous plate model.

Key words: intraplate deformation, plate boundaries, plate tectonics, toroidal–poloidal partitioning.

1 INTRODUCTION

The theories of mantle dynamics and plate tectonics are fundamentally incompatible; the former employs continuum physics while the latter assumes that plates move as rigid bodies and thereby have infinitesimally thin margins. This disparity hampers efforts to couple plate and mantle theories, causing two problems in particular. First, the discontinuity between plates causes plate traction on the mantle to be infinite (Hager & O'Connell 1981). Second, the same discontinuity causes the vorticity (strike-slip shear) and divergence (which represents sources and sinks of mass in the lithosphere) fields to be comprised of unphysical and mathematically intractable singularities (Bercovici & Wessel 1994; Bercovici 1995a). The Earth's plates are for the most part not discontinuous, that is intraplate deformation is common and many

* Now at: Department of Geology, Ecole Normale Superieure, 24 Rue Lhomond, Paris, 75005 France.
† All correspondence.

GJI000 21/4/98 07:13:53 3B2 version 5.20
The Charlesworth Group, Huddersfield 01484 517077

plate margins have significant widths. Thus, efforts to understand how plates are coupled to or generated from mantle flow should not seek to achieve discontinuous plates; such plates are abstractions based on the simple assumptions of the standard plate model, and are therefore unrealistic as well as unrealizable. However, the actual continuity of plates needs to be assessed, and then incorporated into a global plate model; the resulting model would be more compatible with mantle flow models, and represent a more realistic goal for plate-generation theories.

To this end, we here extend the continuous kinematic plate model of Bercovici & Wessel (1994), which introduced finite margin widths into a global model of plate motions. In particular, we use analytically continuous (i.e. infinitely differentiable) functions to describe both plate geometry and plate-margin width. In this paper, the mathematical model of the plate geometries is considerably refined to prevent the excessive smoothing of plate boundaries used by Bercovici & Wessel (1994). Moreover, we demonstrate how geophysical data on intraplate deformation can be incorporated into the model to constrain plate-margin widths; for purposes of demonstration, we use, as an example data set, the global seismicity distribution. This leads to a marked improvement over the *ad hoc* constant margin width assumed in the standard plate model, or in the simple model of Bercovici & Wessel (1994). We refer to this seismicity-based application of the model as the SEISMAR (*seis*micity-inferred *mar*gin-width) plate model. The SEISMAR model of continuous plate motions introduced here is a basic example of how data on intraplate deformation can be incorporated into a global plate-tectonic model.

In this paper we will first present the theoretical model for representing plate shapes and, in particular, develop the necessary improvements to facilitate more realistic plate boundaries. We will then discuss how margin width is determined, for example from global seismicity. Finally, we will examine the implications of the resulting seismicity-based SEISMAR model on global velocity, in particular the associated deformation fields (vorticity and divergence) and kinetic energy partitioning between toroidal and poloidal parts.

2 PLATE SHAPES AND BOUNDARIES

The analysis of how to represent the shape of a tectonic plate with an analytically continuous function is discussed in detail in Bercovici & Wessel (1994). We will here review the more salient points of the theory and explain in detail when we have differed from or improved on that earlier work.

The horizontal velocity field of the Earth's surface, given the motion of N tectonic plates, can be written in a single equation:

$$\mathbf{v} = -\mathbf{R} \times \sum_{i=1}^{N} \mathbf{\Omega}_i S_i(\phi, \theta), \tag{1}$$

where $\mathbf{R}$ is the position vector of a point on the surface of the Earth, at longitude ϕ and latitude θ, and $\mathbf{\Omega}_i$ and S_i are the angular velocity vector and shape function of the ith plate, respectively. The angular velocities of the present-day plates are determined from the NUVEL-1A Pacific-plate-fixed Euler poles (DeMets *et al.* 1994) added to estimates of the instantaneous Pacific hotspot pole from Pollitz's (1988) joint inversion of North American and Pacific plate motions. The shape function S_i is defined to be 1 within the plate and 0 outside the plate. For the standard plate model, S_i has a discontinuous transition from 1 to 0, whereas the transition is continuous and smooth (i.e. infinitely differentiable) in the continuous model. The procedure for determining S_i in the continuous model requires several steps as discussed below (see also Bercovici & Wessel 1994).

2.1 Plate-boundary filtering.

To make the model of the tectonic plates analytically continuous, the plate boundaries must be smoothed at least slightly to remove minor discontinuities (e.g. ridge–transform offsets). This is necessary to allow the boundary to be modelled as a mathematically single-valued function (see next subsection). In Bercovici & Wessel (1994), smoothing was performed until each plate boundary could be represented as a single-valued polar function in which the polar origin was at some point inside the plate. To that end, a very large filter width [7000 km Gaussian full-width; see Bercovici & Wessel (1994)] was necessary so that the most non-circular plates (for example nearly horse-shoe-shaped ones such as the Austro–Indian plate) could be sufficiently rounded out. Invariably, each resulting smoothed plate became a crude first-order representation of the original plate, and smaller plates, such as the Cocos plate (with its lopsided hour-glass shape), became almost entirely circularized. However, to employ data on intraplate deformation (such as seismicity) to estimate margin widths, it is necessary that the zones of high deformation (e.g. dense seismicity) coincide accurately with the plate boundaries. Therefore, to preserve plate-boundary structures we use a much finer filter width (1000 km Gaussian full-width); the original and smoothed (filtered) plate shapes are shown in Fig. 1. To represent the plate boundaries with single-valued functions therefore requires additional manipulation, as discussed below.

2.2 Plate division

We begin with the 13 major tectonic plates of the Earth as listed in DeMets *et al.* (1990, 1994). The Australian and Indian plates are divided along their diffuse margin as indicated by Wiens *et al.* (1985) (Figs 1 and 2). The actual dividing line is a linear function of longitude ϕ and latitude θ, that is a straight line in a cylindrical equirectangular projection (in which longitude and latitude are essentially treated as Cartesian coordinates); the endpoints to this line are $\phi_1 = 68.4$, $\theta_1 = -6.6$ and $\phi_2 = 95.4$, $\theta_2 = 2.2$.

With the finer smoothing employed in this paper, it is not possible for each plate boundary to be automatically represented with a single-valued function. Thus it is necessary to subdivide further several plates along arbitrary pseudo-boundaries. These pseudo-boundaries are chosen to maximize the circularity of the resulting subplates; for example, a horseshoe-shaped plate would be divided across its centre curve, while an hour-glass-shaped plate would be divided along its neck. In some cases, it is necessary to divide particularly large plates into three and four subplates. To ensure that the pseudo-boundaries do not significantly influence the final

GJI000 21/4/98 07:14:35 3B2 version 5.20
The Charlesworth Group, Huddersfield 01484 517077

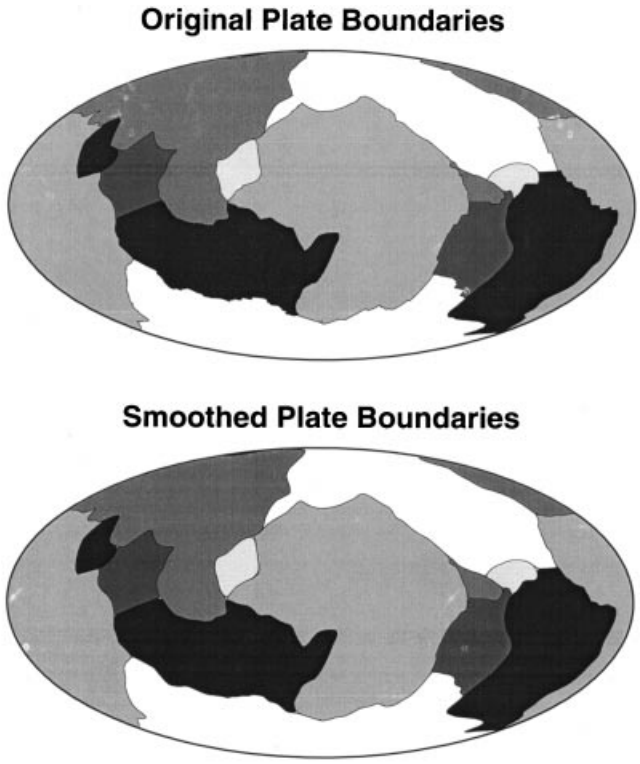

Figure 1. Original plate boundaries (top) and the same plate boundaries smoothed with a 1000 km Gaussian full-width filter (bottom), as employed in the continuous plate model.

model, it is necessary that a subplate and its complement (that is the adjacent subplate sharing the common pseudo-boundary) fit precisely back together. This is discussed in more detail in Section 3.3.

Plate divisions near the equator are made by pseudo-boundaries that are simply straight lines in an equirectangular projection (that is θ is a linear function of ϕ). However (as discussed below), the plate-boundary function for a given plate is found in a frame of reference for which that plate does not contain a geographic pole and is far from the zero meridian (to avoid discontinuous changes in longitude), that is each subplate is moved to a frame such that its effective centre of mass is near the equator and the 180° meridian (see Bercovici & Wessel 1994). However, pseudo-boundaries located at high latitudes can undergo significant distortion when being rotated to the equator; thus to preserve the simplicity of these pseudo-boundaries on rotation, they are determined by great circles with specified endpoints. Information on all pseudo-boundaries is given in Table 1 (that is the plate it divides, its endpoints, and the type of boundary, either a straight line in an equirectangular projection or a great circle). The straight-line pseudo-boundaries are defined by

$$\theta_{\mathrm{pb}} = a\phi + b \tag{2}$$

(where a and b are determined such that the line has endpoints as listed in Table 1). The great-circle pseudo-boundaries are given by

$$\theta_{\mathrm{pb}} = \tan^{-1}(a\cos\phi + b\sin\phi), \tag{3}$$

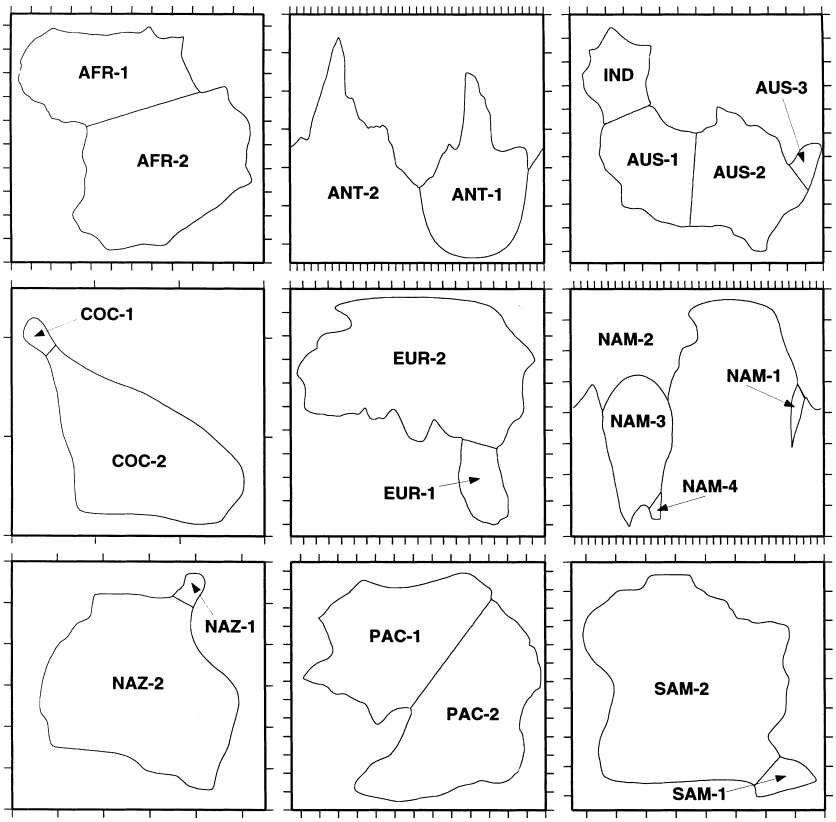

Figure 2. Plates divided by pseudo-boundaries (with labelled subplates).

GJI000 21/4/98 07:14:56 3B2 version 5.20
The Charlesworth Group, Huddersfield 01484 517077

Table 1. Pseudo-boundary information.

Plate	ϕ_1 (deg)	θ_1 (deg)	ϕ_2 (deg)	θ_2 (deg)	Boundary type
African	43.7231	12.1501	−12.1895	−2.6453	straight line
Antarctic	183.3320	−65.3357	338.0790	−60.4307	great circle
Australian	16.0360	−49.3737	119.6860	−10.0926	straight line
	181.5650	−34.3662	170.8820	−23.3943	straight line
Cocos	254.1260	18.1296	255.3420	19.2305	straight line
Eurasian	122.1750	22.2206	94.9668	26.3249	straight line
Nazca	275.0440	1.6506	279.5100	−1.0551	straight line
N. American	162.3830	54.5400	152.0150	59.3193	straight line
	−62.4904	18.9033	−45.1415	24.3281	straight line
	−34.6069	53.8276	129.1240	50.1203	great circle
Pacific	188.2280	−14.7373	231.3450	44.8559	straight line
S. American	336.1190	−56.6925	344.8290	−46.6037	straight line

where a and b in this case are defined such that the pseudo-boundary is the intersection of the surface of the Earth with the plane $z=ax+by$ [where $(x, y, z)=|\mathbf{R}|(\cos\theta\cos\phi, \cos\theta\sin\phi, \sin\theta)$] that passes through the centre of the Earth and the endpoints listed in Table 1. All divided plates are shown individually in Fig. 2; the subplates are also labelled to facilitate further discussion.

2.3 The boundary function

As stated above and in Bercovici & Wessel (1994), each plate or subplate is rotated to a frame of reference where its centre is at a longitude of 180° and latitude of 0°. (The centre of the plate is defined as its effective centre of mass wherein equal masses are placed at evenly spaced distances along the boundary.) The coordinates of this frame of reference are denoted as (ϕ', θ'). For a given plate the pseudo-distance from an arbitrary point within the plate (ϕ'_o, θ'_o) to any other point on the globe (ϕ', θ') is

$$\Delta(\phi', \theta')=\sqrt{(\phi'-\phi'_o)^2+(\theta'-\theta'_o)^2}\,. \tag{4}$$

The pseudo-angle between the line connecting these two points and the line connecting (ϕ'_o, θ'_o) to the first plate-boundary data point $(\phi'_{b_1}, \theta'_{b_1})$ is

$$\alpha=\tan^{-1}\left(\frac{\theta'-\theta'_o}{\phi'-\phi'_o}\right)-\tan^{-1}\left(\frac{\theta'_{b_1}-\theta'_o}{\phi'_{b_1}-\phi'_o}\right). \tag{5}$$

[The terms 'pseudo-distance' and 'pseudo-angle' are used because these quantities treat θ' and ϕ' as if they were Cartesian coordinates; see Bercovici & Wessel (1994).] An arbitrary boundary point (ϕ'_b, θ'_b) has pseudo-distance $\Delta_b=\Delta(\phi'_b, \theta'_b)$. In order to make the plate shape analytically continuous, Δ_b must be expressed as a single-valued function of α; this function $\Delta_b(\alpha)$ is called the *plate-boundary function*. Achieving a single-valued $\Delta_b(\alpha)$ requires a prudent choice of the polar origin (ϕ'_o, θ'_o). Here, the optimum (ϕ'_o, θ'_o) yields the smallest maximum value of $|d\Delta_b/d\alpha|$ since this would be zero for the ideal circular boundary while a multivalued $\Delta_b(\alpha)$ would have singularities in its slope. The optimum values of ϕ'_o and θ'_o are found numerically for all 25 plates and/or subplates. Since most plates and subplates are, to first order, elliptically shaped, most of the (ϕ'_o, θ'_o) are near (180, 0). Table 2 shows the values of (ϕ'_o, θ'_o) for each plate or subplate (see Fig. 2 for subplate labels).

Table 2. Polar coordinate origin (ϕ'_o, θ'_o) for each plate and subplate.

Plate	ϕ'_o (deg)	θ'_o (deg)
African-1	187.02	−13.06
African-2	175.50	−13.06
Antarctic-1	185.06	−0.39
Antarctic-2	158.77	−24.49
Arabian	177.24	−4.63
Australian-1	180.66	−0.59
Australian-2	182.97	2.94
Australian-3	178.83	−0.87
Carribean	181.92	0.95
Cocos-1	180.26	−0.52
Cocos-2	174.86	3.67
Eurasian-1	181.06	0.79
Eurasian-2	174.28	3.25
Indian	178.35	−3.39
Nazca-1	180.12	−0.41
Nazca-2	184.11	7.47
N. American-1	180.71	2.67
N. American-2	182.04	−9.33
N. American-3	158.44	4.64
N. American-4	180.06	−1.64
Pacific-1	187.08	−17.05
Pacific-2	194.28	4.53
Philippine	178.50	−1.44
S. American-1	179.60	0.69
S. American-2	190.59	−9.68

The plate-boundary function $\Delta_b(\alpha)$ is therefore constructed from all the points on the boundary; it is then evenly resampled in α with radix-2 number of points and discrete Fourier transformed to obtain

$$\Delta_b(\alpha)=\frac{1}{N}\sum_{n=-N/2}^{N/2}\Delta_b^{(n)}\,e^{in\alpha}\,, \tag{6}$$

where N is the number of resampled points. In this way, $\Delta_b(\alpha)$ is expressed as an analytic function.

2.4 Plate-shape and plate-margin functions

Given the plate-boundary function $\Delta_b(\alpha)$, the plate shape function S of any given plate is

$$S(\phi', \theta')=\frac{1}{2}\left[1+\tanh\left(\frac{\Delta_b(\alpha)-\Delta}{\delta^*(\alpha)}\right)\right], \tag{7}$$

GJI000 21/4/98 07:15:10 3B2 version 5.20
The Charlesworth Group, Huddersfield 01484 517077

where δ^* is the plate-margin half-width (in the pseudo-coordinates employed here) along the line connecting the points (θ'_o, ϕ'_o) and (θ', ϕ'); *δ^* is not the margin half-width normal to the boundary*. The plate-margin function δ^* is the crucial addition to the plate-tectonic model since it incorporates information about margin width and intraplate deformation. How this function is determined is demonstrated in the following section.

3 THE SEISMAR MODEL: A SEISMICITY-BASED EXAMPLE

Here we illustrate how the margin width function δ^* is determined via geophysical data on intraplate deformation. A variety of data sets could be used to estimate δ^*, including for example global seismicity, stress distributions (Zoback & Burke 1993), fault distributions, and possibly a variant of gravity and bathymetry (Smith & Sandwell 1994; Sandwell & Smith 1997). While no one data set is clearly preferable, in this paper we employ seismicity for the sake of demonstration, for its utility and accessibility, and because it is the classic delineator of tectonic boundaries. Since the plate-margin function is only meant to indicate the presence of (and not amount or force of) deformation, the seismicity data is not weighted, for example by earthquake moment or magnitude, which contains information about the amount of displacement along with crustal/lithosphere strength, etc. The use of geologically recent seismicity data of course gives a very current estimate of plate-margin structure and thus is relevant for models (e.g. mantle flow models) which need to employ instantaneous motion. We discuss below how the data are chosen, used and manipulated in order to yield the plate-margin function δ^*. We refer to the resulting seismicity based application as the SEISMAR plate model.

3.1 The seismicity data

We use seismicity data for the period from 1928 to 1990 in the June 1992 version of the Global Hypocenter Data Base. While earthquake locations are less reliable prior to 1960, we choose to have a large data set to facilitate resolution of plate margins (that is to minimize gaps in seismicity along plate boundaries). Certain constraints, however, are placed on the chosen earthquakes. First, we allow only earthquakes whose focal depth is less than or equal to 29 km; this is done because indeterminate focal depths are, by default, assigned a value of 30 km (F. Duennebier, personal communication, 1996). Earthquakes deeper than 30 km are eliminated as they are less representative of plate-boundary deformation and interactions (and are liable to be influenced by deep earthquakes which are well removed from plate boundaries). We also choose only earthquakes with magnitude greater than 4 (given that small earthquakes have poorly determined locations). Finally, we obtain the locations of 24 721 earthquakes (Fig. 3). However, when necessary we delete intraplate earthquakes that are clearly unrelated to plate deformation (for example earthquakes on Hawaii which are primarily from landslides and volcanic activity).

3.2 Determination of margin widths

For a given plate we consider only the subset of the seismicity data which includes (1) earthquakes on the plate itself, and (2) earthquakes outside the plate but within 500 km of the plate boundary (and not including earthquakes associated with other plate boundaries). We then calculate the position of each earthquake in terms of the pseudo-distance Δ and angle α.

We next divide the given plate into wedges of equal angular extent $d\alpha$ and bin the seismicity data on each wedge (Fig. 4). Thus the number of earthquakes N_{eq} at pseudo-distance Δ and a given α is in fact the number of earthquakes at Δ between $\alpha - d\alpha/2$ and $\alpha + d\alpha/2$ (Fig. 4). If N_{eq} versus Δ at the given α had a normal (Gaussian) distribution centred at $\Delta = \Delta_b$, then the margin half-width would be the Gaussian half-width (that is $\sqrt{2}$ times the standard deviation) of the distribution. However, given the scatter and occurrence of outliers in the actual data, we employ robust estimation techniques (Rousseeuw & Leroy 1987) and define the margin width as the minimum width of the window (in the units of pseudo-distance) which contains 50 per cent of the earthquakes (again, in the wedge centred on α). (This step is considerably facilitated if one first sorts the earthquake location in each wedge in order of increasing Δ.) By finding this width for each α we build the raw margin function $\delta^*_o(\alpha)$ (deemed raw as it still requires some additional processing, as discussed below).

The chosen wedge size $d\alpha$ differs between plates because, for example, the $d\alpha$ for a small plate is larger than that for a big plate since the smaller plate is likely to have fewer earthquakes

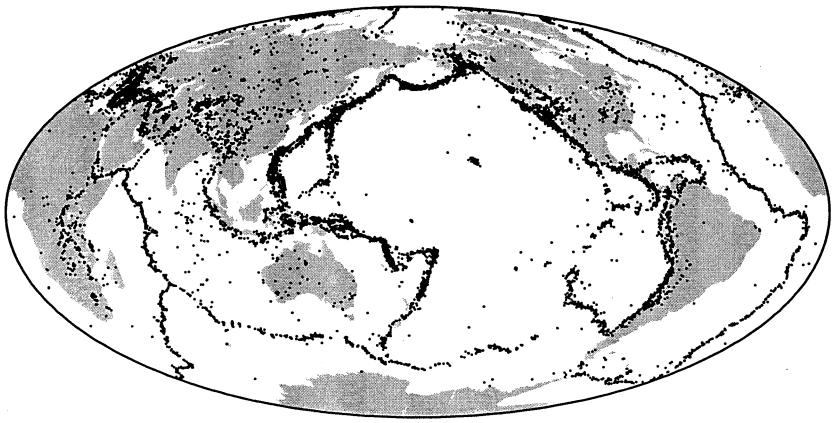

Figure 3. Global seismicity distribution used to determine plate-margin widths.

GJI000 21/4/98 07:15:41 3B2 version 5.20
The Charlesworth Group, Huddersfield 01484 517077

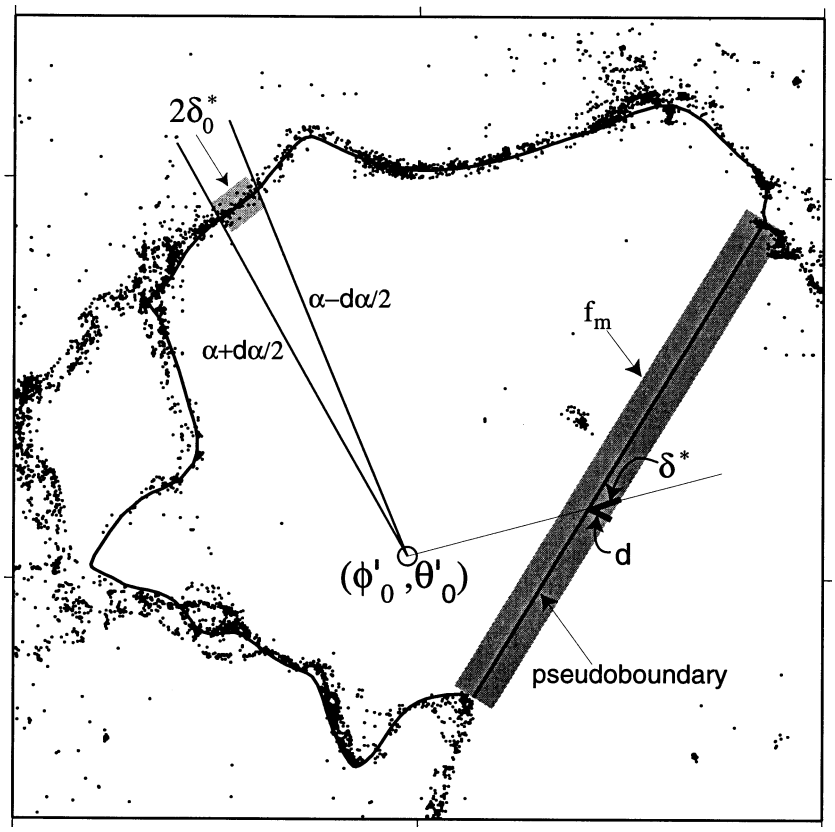

Figure 4. Sketch illustrating the determination of margin width along the true boundary and pseudo-boundary of a single subplate, in this case the northern Pacific plate (Pacific-1, see Fig. 2). On the true boundary, the oblique margin width at angle α is determined by binning the seismicity within a wedge between $\alpha - d\alpha/2$ and $\alpha + d\alpha/2$ (upper left); the margin is then the narrowest region which contains 50 per cent of the earthquakes in that wedge (the shaded region, which is exaggerated for the sake of clarity). The margin width of the pseudo-boundary (lower right) is found by measuring, along a line of constant α, the width of a box-car function f_m centred on the boundary (long shaded region). The figure, however, is over-simplified and should only be considered illustrative; in particular, f_m is defined in the original coordinate frame (ϕ, θ), while the measurements of margin width are carried out in the rotated frame (ϕ', θ'). See text for further discussion.

along its boundary. In general we use between 60 and 70 wedges for the bigger plates, and 20 to 30 for the smaller ones. Moreover, we can only calculate a margin width in a wedge if it has more than four earthquakes. If there are fewer than four earthquakes in the wedge we assume the margin width is the average of the widths from the two surrounding wedges.

To determine the confidence in the inferred margin width, we also record the total number of earthquakes on each wedge $M(\alpha)$. We then smooth the function $\delta_o^*(\alpha)$ by a Gaussian filter that is weighted by $M(\alpha)$; in this way values of δ_o^* that have higher confidence are more strongly weighted. [The Gaussian filter is arbitrarily chosen to have a half-width that is $(3/2)d\alpha$]. Therefore, our smoothed margin width at the ith value of α is

$$\delta^*(\alpha_i) = \frac{\sum_j \delta_o^*(\alpha_j) M(\alpha_j)\, e^{-(\alpha_j-\alpha_i)^2/(3/2d\alpha)^2}}{\sum_j M(\alpha_j)\, e^{-(\alpha_j-\alpha_i)^2/(3/2d\alpha)^2}} . \quad (8)$$

However, the pseudo-boundaries (where some plates are divided) must be left intact so the parts of a plate will fit back together again along the boundary as tightly as possible. The calculation of the margin widths for the pseudo-boundaries is discussed below.

As with the boundary function $\Delta_b(\alpha)$, the margin function can be put into an analytic form with discrete Fourier transforms, though since δ^* is defined only on wedges and not each boundary point, it is defined (usually resampled to radix 2 points) at fewer values of α.

3.3 Pseudo-boundary margin widths

The creation of pseudo-boundaries has no (or negligible) effect on the final model of plate kinematics as long as the effects of these boundaries' margins essentially cancel each other once all the subplates are pieced back together again. The shape functions of a subplate and its complement (that is the adjacent subplate sharing the pseudo-boundary) should add to unity on the pseudo-boundary. As a simple example, the 1-D hyperbolic-tangent step function (centred at $x = x_o$ and of margin width δ) and its mirror image add to unity:

$$\frac{1}{2}\left[1 + \tanh\left(\frac{x-x_o}{\delta}\right)\right] + \frac{1}{2}\left[1 - \tanh\left(\frac{x-x_o}{\delta}\right)\right] = 1 . \quad (9)$$

However, these functions only add to unity as long as they each have the same margin width. Moreover, since complementary subplates have the same Euler pole, there is no differential

GJI000 21/4/98 07:16:12 3B2 version 5.20
The Charlesworth Group, Huddersfield 01484 517077

motion across their pseudo-boundary and thus the pseudo-boundary has little or no effect on strain-rate, vorticity and divergence fields.

However, the actual description of margin widths on pseudo-boundaries is not as precise or as simple as implied by (9) given that the boundaries are arbitrary curves on a spherical surface, and the margin widths are measured from completely different points on a subplate and its complement.

To make a subplate and its complement fit as tightly as possible along a pseudo-boundary the definition of the margin must be precise. The margin width must have a consistent mathematical definition that is frame-invariant (in particular-independent of the frame of reference of the subplate in which the margin width is measured). Thus, it is best to have an exact mathematical description of the margin in the original spherical coordinates ϕ and θ. For precision we delineate the margin region of the plate with a top-hat or box-car function centred along the pseudo-boundary, representing, say, a distribution of fictional earthquakes (see Fig. 4); that is this function is 1 inside and 0 outside the margin region. Since a pseudo-boundary curve is given by the single-valued function $\theta_{pb}(\phi)$ (see eqs 2 and 3), the margin region is therefore defined by the function

$$f_{\mathrm{m}}(\phi, \theta) = \frac{1}{2}\left[1 + \mathrm{sgn}\left(1 - \left(\frac{\theta - \theta_{pb}(\phi)}{\delta(\phi)}\right)^2\right)\right], \tag{10}$$

where $\delta(\phi)$ is the margin half-width measured in the north–south direction. For simplicity, we prescribe the margin to have a constant half-width d normal to the boundary (see Fig. 4) and thus

$$\delta(\phi) = d\sqrt{1 + \left(\frac{d\theta_{pb}}{d\phi}\right)^2} \tag{11}$$

[that is $\delta = d$ if the boundary at that particular ϕ is tangent to an east–west line, and $\delta \to \infty$ if the boundary approaches a north–south tangent; see also Bercovici & Wessel (1994)]. With this definition, the margin width measured from the centres of two adjacent subplates will be derived from the same formula.

With the margin region for a given plate's pseudo-boundary defined in the (ϕ, θ) coordinate system, we need to measure the width of the region in the rotated polar coordinate system (Δ, α). For a given constant-α line (that intersects the pseudo-boundary) the values of f_{m} are calculated for increasing Δ [using in (10) the ϕ and θ uniquely corresponding to the given Δ and α]. The margin half-width along this constant α line is thus

$$\delta^* = \frac{1}{2}\left(\Delta_{\max} - \Delta_{\min}\right), \tag{12}$$

where $\Delta_{\min}$ and $\Delta_{\max}$ are, respectively, the minimum and maximum Δ for which $f_{\mathrm{m}} = 1$. (Precise measurement of δ^* may require many incremental steps in Δ to resolve properly the margin region, sometimes as many as 50 000 steps.) This is done for a sufficient number of α along the pseudo-boundary (typically about 20 values). In this way we obtain a sampling of the function $\delta^*(\alpha)$ along the pseudo-boundary. This sampling is appended to the filtered sampling of $\delta^*(\alpha)$ along the true boundaries (with seismicity data) to yield a complete margin function $\delta^*(\alpha)$ for $0 \le \alpha \le 2\pi$. Incorporation of the total margin function for each plate into the associated plate shape function (see eq. 7) comprises the essential part of the SEISMAR plate model.

Fig. 5 shows an example of the seismically inferred margin width for a plate with considerable variability in its margin structure, that is the Eurasian plate. Where the concentration of earthquakes is dense the margin width is relatively narrow and well defined. However, where earthquakes are poorly concentrated, the margin width is appropriately broad (for example the northeastern margin of the Eurasian plate).

4 RESULTS OF THE SEISMAR MODEL

4.1 Divergence and vorticity fields

The Earth's plate motions can be divided linearly into poloidal and toroidal parts (Hager & O'Connell 1978, 1979). Poloidal flow represents divergent motion (ridges and subduction zones) and thus reflects upwelling and downwelling in the mantle. Toroidal motion represents purely horizontal rotational motion as exists in the spin of plates and strike-slip shear. Poloidal motion is typical of convective flow. However, the issue of how and why the purely horizontal and dissipative toroidal motion is generated in the plate-mantle system remains a fundamental, yet largely unresolved, aspect of our understanding of how plate tectonics is linked to mantle convection (see Bercovici 1993, 1995a,b, 1996, 1998; Zhong & Gurnis 1995a,b, 1996).

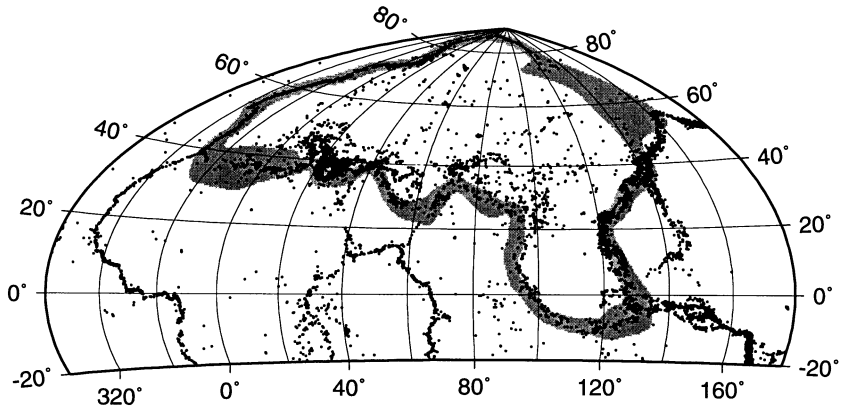

Figure 5. The seismically inferred margin width for the Eurasian plate, superimposed on the local seismicity distribution. The plot shows the shape function S for the entire Eurasian plate; however, only values between $S = 0.1$ and 0.9 are given a single grey shade, while all other values are white.

In this section we show how the SEISMAR model resolves the poloidal and toroidal parts of the Earth's present-day plate motions. In particular, we will examine the horizontal divergence and vertical vorticity of the plate motions which are the most detailed manifestations of the poloidal and toroidal fields. In the standard plate model divergence and vorticity are essentially impossible to resolve as they are singularities (due to the assumption of zero margin width). However, in the continuous plate model, and the SEISMAR model in this paper, these quantities are quite resolvable and contain considerable detail about deformation of the Earth's surface. Although this model also has certain drawbacks and artefacts it gives us the first quantitative estimate of the Earth's surface divergence and vorticity fields.

4.1.1 Theoretical background

The 2-D velocity on the surface of a sphere can be expressed with a Helmholtz representation:

$$\mathbf{v} = \nabla\Phi + \nabla \times (\hat{r}\Psi), \tag{13}$$

where ∇ is the horizontal gradient, Φ is the poloidal potential, Ψ is the toroidal stream function, and $\hat{r}$ is the unit vector in the radial direction. Horizontal divergence is

$$D = \nabla \cdot \mathbf{v} = \nabla^2\Phi, \tag{14}$$

while radial or vertical vorticity is

$$\omega_r = \hat{r} \cdot \nabla \times \mathbf{v} = -\nabla^2\Psi. \tag{15}$$

Divergence and vorticity are thus also representative of the poloidal and toroidal fields, respectively. However, since the divergence and vorticity involve gradients of Φ and Ψ, they enhance the finer small-scale features and thus permit a more detailed description of the poloidal and toroidal fields.

To calculate the divergence and vorticity fields directly we would simply find the appropriate horizontal gradients of the surface velocity field. This is possible in the continuous plate model, but not so in the standard plate model. In the continuous plate model we would obtain the following [from substituting (1) into (14) and (15)]:

$$D = -\sum_{i=1}^{N} \Omega_\phi^{(i)} \frac{\partial S_i}{\partial \theta} + \Omega_\theta^{(i)} \frac{1}{\cos\theta} \frac{\partial S_i}{\partial \phi}, \tag{16}$$

$$\omega_r = \sum_{i=1}^{N} 2 S_i \Omega_r^{(i)} + \Omega_\theta^{(i)} \frac{\partial S_i}{\partial \theta} - \Omega_\phi^{(i)} \frac{1}{\cos\theta} \frac{\partial S_i}{\partial \phi}, \tag{17}$$

where

$$\Omega_r^{(i)} = (\Omega_x^{(i)} \cos\phi + \Omega_y^{(i)} \sin\phi)\cos\theta + \Omega_z^{(i)} \sin\theta, \tag{18}$$

$$\Omega_\theta^{(i)} = (\Omega_x^{(i)} \cos\phi + \Omega_y^{(i)} \sin\phi)\sin\theta - \Omega_z^{(i)} \cos\theta, \tag{19}$$

$$\Omega_\phi^{(i)} = \Omega_y^{(i)} \cos\phi - \Omega_x^{(i)} \sin\phi, \tag{20}$$

and $\mathbf{\Omega}_i = (\Omega_x^{(i)}, \Omega_y^{(i)}, \Omega_z^{(i)})$. Since the plate margins for the continuous plate model are of finite width, the various derivatives of S_i are calculable. Moreover, since D and ω_r are scalars they are invariants and thus we need only determine them for each individual plate or subplate in the plate's specific plate-centred reference frame (ϕ', θ'). Both divergence and vorticity involve derivatives of each plate's shape function S with respect to ϕ' and θ'; these take the form

$$\frac{\partial S}{\partial \chi^\pm} = \pm \frac{1}{2\delta^*} \operatorname{sech}^2\left(\frac{\Delta_b - \Delta}{\delta^*}\right) \frac{\chi^\mp - \chi_o^\mp}{\Delta^2} \times \left[\frac{d\Delta_b}{d\alpha} \mp \left(\frac{\chi^\pm - \chi_o^\pm}{\chi^\mp - \chi_o^\mp}\right)^{\pm 1} \Delta - (\Delta_b - \Delta) \frac{d \ln \delta^*}{d\alpha}\right], \tag{21}$$

where $\chi^+ = \theta'$, $\chi^- = \phi'$ and we use Fourier transforms of Δ_b and δ^* to evaluate their derivatives with respect to α. Although these derivatives are susceptible to Gibbs effects, such effects can be reduced with modest Gaussian filtering in the Fourier domain (see Bercovici & Wessel 1994). We then simply use the value of D or ω_r at the point (ϕ', θ') for the divergence and vorticity of the associated point (ϕ, θ). The D and ω_r for all the plates are then added together to yield the total divergence and vorticity fields.

For the standard plate model the shape function S is essentially constructed from discontinuous step functions and therefore derivatives of S do not exist (that is they are singularities). One can, however, determine the divergence and vorticity from the velocity field without taking gradients of $\mathbf{v}$. This method involves vector spherical harmonic transforms (see O'Connell, Gable & Hager 1991) and yields the spherical harmonic transform of D and ω_r, not the physical quantities themselves. Using this method one finds that the spherical harmonic transforms of D and ω_r are

$$D_{lm} = -\int_{4\pi} \nabla Y_l^{m^*} \cdot \mathbf{v} d\Omega, \tag{22}$$

$$\omega_{lm} = -\int_{4\pi} \nabla \times (\hat{r} Y_l^{m^*}) \cdot \mathbf{v} d\Omega, \tag{23}$$

where Ω is the solid angle, and $Y_l^{m^*}$ is the complex conjugate of the normalized spherical harmonic Y_l^m of degree l and order m. In this way divergence and vorticity can be calculated from the expansions

$$D = \sum_{l=1}^{L} \sum_{m=-l}^{+l} D_{lm} Y_l^m, \tag{24}$$

$$\omega_r = \sum_{l=1}^{L} \sum_{m=-l}^{+l} \omega_{lm} Y_l^m, \tag{25}$$

where L is the maximum l used.

4.1.2 Field representations

The divergence and vorticity fields for the standard discontinuous plate model (using 22–25 with $L = 40$; O'Connell, personal communication, 1992) are shown in Fig. 6. Even though the vector spherical harmonic transforms from which these are derived do not directly involve singularities, the divergence and vorticity fields for this model are intrinsically singular. This causes the excessive ringing or Gibbs phenomenon extant in both fields. Moreover, the magnitudes of D and ω_r depend on L, that is where the spherical harmonic series is truncated. Some of the broader true features are discernible in the divergence and vorticity fields, such as the East Pacific Rise, and the Southeast Indian Ridge. However, the Gibbs effect obscures any finer or more complex features, such as those around the Philippine plate. Finally, it is worth noting for the sake of later comparison that

GJI000 21/4/98 07:17:00 3B2 version 5.20
The Charlesworth Group, Huddersfield 01484 517077

the divergence field has the largest amplitude feature which occurs the along East Pacific Rise. The maximum vorticity is about 80 per cent of the maximum divergence and occurs on the southwest side of the Philippine plate (though the structure of the entire Philippine plate is obscured by ringing).

The divergence and vorticity fields for the continuous, SEISMAR plate model (using 16 and 17) are shown in Fig. 7. Since these fields are calculated directly, that is without spectral transforms, they exhibit no ringing. While the SEISMAR model does yield some artefacts (discussed below), it also gives a detailed picture of D and ω_r, clearly showing the effects of even the smallest plates. The magnitudes of the divergence and the vorticity fields are not artefacts of the model resolution but arise from the Euler pole and seismicity data. Thus the SEISMAR model gives the first quantitative estimate of the strengths of these fields.

Fine details of the divergence and vorticity fields can be resolved with the SEISMAR model that cannot be distinguished with the standard model. For example, the small positive divergence embedded in a convergent zone near the southeastern boundary of the Philippine plate is indicative of the Ayu trough (Weissel 1980); this feature would not be permitted in the standard model since it would be cancelled out by the negative divergence of the Yap and Marianas trenches.

In the SEISMAR model the vorticity field has the largest maximum near the northern end of the East Pacific Rise, not near the Philippine plate as implied with the standard plate model. However, two distinct local maxima in the vorticity field occur on the northern and southern corners of the Philippine plate. The maximum positive divergence also occurs on the East Pacific rise, as with the standard model. However, the maximum absolute divergence is in fact negative, in contrast to the standard model.

Of particular interest is the effect of broad plate margins. One can distinctly see that the northeastern boundary of the Eurasian plate, which hypothetically cuts across a diffuse seismicity zone in Siberia, is hardly manifested at all in the divergence and vorticity fields; this is entirely due to the breadth of the margin as estimated from the widely and sparsely distributed seismicity data. Moreover, the distribution of seismicity in the Basin and Range province causes the vorticity field over the San Andreas region to be well defined but relatively broad. One can also discern, in both the divergence and vorticity fields, the effect of the diffuse boundary separating the Australian and Indian plates.

Finally, the SEISMAR model clearly shows shades of non-zero vorticity permeating some plate interiors (for example the Pacific, Philippine and especially the Cocos plates). This effect is the direct consequence of plate spin, which is proportional to plate area, and not deformation on the margins (see the first term in 17).

4.1.3 Artefacts of the SEISMAR model

Although the SEISMAR model creates a relatively clear and quantifiable representation of the Earth's divergence and vorticity fields, it also creates some minor artefacts that are worthy of discussion. Foremost is that the pseudo-boundaries show a very small but discernible signature in the divergence and vorticity fields. In particular one can observe slight seams in most of the larger plates (for example the seam running southwest–northeast in the Pacific plate). (These seams are also emphasized in the figures due to the false illumination projected from the southwest.) In the plate interiors these seams are not strong enough to register outside the narrow zero-centred grey range (that is less than 5 per cent of the maximum) of the colour scale in Figs 6 and 7; however, they do manifest themselves more distinctly where they intersect a true boundary. Although these artefacts are second order at worst, they demonstrate that there is room for improvement in the continuous plate model, or in the application of seismicity in the SEISMAR model. While considerable care was taken to resolve accurately the pseudo-boundaries (so that sections of a divided plate would fit cleanly together again) there are still some problems. First, pseudo-boundaries (both the boundary distance and margin width) are not sampled by two adjacent plates from the same coordinate system; thus the boundary shape and width are not measured at the same points or from the same angles by two complementary plates. This scheme for sampling the pseudo-boundaries might be made more exact in future studies. Alternatively, it may be possible to apply essentially a high-pass filter to the divergence and vorticity fields, that is permit only values with absolute values greater than some minimum and thus effectively exclude most of the effects of the pseudo-boundaries. This latter method is arbitrary at best and thus not entirely satisfactory.

Another artefact of the SEISMAR model is evident in the spikes and ringing in the divergence and vorticity fields along (that is parallel to) the margins. This undoubtedly occurs because of the often highly oscillatory nature of the margin width function $\delta^*(\alpha)$ for many plates. This in itself probably reflects the sparse coverage of seismicity data on certain plate boundaries and/or diffuse boundaries. Even with smoothing weighted by confidence [that is number of earthquakes, e.g. from (8)], the resolution of δ^* in α is still relatively coarse in order to permit more than four earthquakes per wedge of the plate; this can cause significant variation from one α to the next, which manifests itself as spikes and some secondary ringing of D and ω_r along the boundaries. Again, these artefacts might be reduced by more aggressive filtering, or by using more data on plate-margin widths (for example other data sets with additional resolution of plate boundaries).

4.2 Power spectra and kinetic energy partitioning

The kinetic energies of toroidal and poloidal motions are mostly dependent on the bulk size and shape of the larger plates, and not extensively on the margin width. Thus one should expect that the toroidal and poloidal kinetic energies, their power spectra and their ratio should differ little from one plate model to the next. We therefore examine the effect (or lack of effect) the SEISMAR model has on the various characteristics of the toroidal and poloidal kinetic energies (as well as the power spectra of the divergence and vorticity fields).

The spherical harmonic kinetic energy spectrum is defined as the kinetic energy for each spherical harmonic degree l; the poloidal and toroidal energy spectra (per unit mass and divided by R^2) are, respectively,

$$KE_{\mathrm{P}}(l) = \frac{1}{2l(l+1)} \sum_{m=-l}^{+l} D_{lm} D_{lm}^{*}, \tag{26}$$

$$KE_{\mathrm{T}}(l) = \frac{1}{2l(l+1)} \sum_{m=-l}^{+l} \omega_{lm} \omega_{lm}^{*}. \tag{27}$$

GJI000 21/4/98 07:17:40 3B2 version 5.20
The Charlesworth Group, Huddersfield 01484 517077

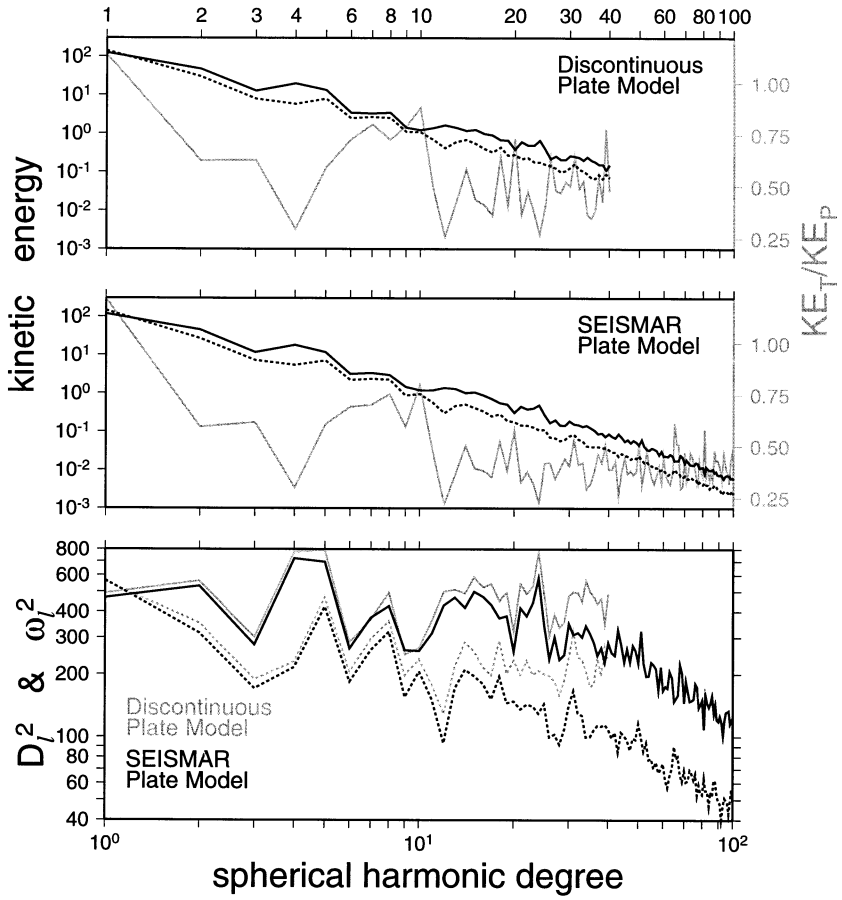

Figure 8. Spherical harmonic spectra for the poloidal (dark solid line) and toroidal (dashed line) kinetic energies, and the ratio of toroidal to poloidal energy (grey solid line) for both the discontinuous and the SEISMAR plate models (top two frames). Spherical harmonic power spectra for horizontal divergence (solid lines) and radial vorticity (dashed lines) for both the standard and the SEISMAR plate models (bottom frame).

Fig. 8 (top two frames) shows these spectra and their ratios for both the standard discontinuous plate model and the SEISMAR model. One can see that the SEISMAR model has little effect on the amplitude and shape of this spectrum, as expected. The ratio of the energies $KE_T(l)/KE_P(l)$ is also shown in the same figure and this emphasizes some minor differences between the two models. The ratio for both models is greater than unity only in the $l=1$ mode, which represents the amount of net lithospheric spin. The ratio is noticeably larger at $l=1$ for the SEISMAR model than for the standard model. Moreover, the local peak in the ratio at $l=39$ in the standard model is not present in the SEISMAR model. These differences may reflect the use of finite margins in the SEISMAR model because, for example, with more diffuse margins the SEISMAR model gives relatively more weight to spin kinetic energy in the toroidal field (which depends on plate area, not on margin structure).

For the standard plate model the total poloidal and toroidal kinetic energies and their ratio are $KE_P=243$ (rad Gyr^{-2}), $KE_T=207$ (rad Gyr^{-2}) and $KE_T/KE_P=0.85$. For the SEISMAR model $KE_P=228$ (rad Gyr^{-2}), $KE_T=202$ (rad Gyr^{-2}) and $KE_T/KE_P=0.88$. The SEISMAR poloidal energy is 6 per cent and the toroidal energy 3 per cent lower than those for the standard model, while the energy ratio is higher for the SEISMAR model. While these differences between the models are subtle, they are systematic and thus probably reflect the reduction in energy associated with deformation on margins in the SEISMAR model, and thus a higher proportion of spin energy in the SEISMAR toroidal field.

A perhaps more revealing power spectra involves the squared amplitude of divergence and vorticity at each spherical harmonic degree, that is

$$D_l^2 = \sum_{m=-l}^{+l} D_{lm} D_{lm}^* , \tag{28}$$

$$\omega_l^2 = \sum_{m=-l}^{+l} \omega_{lm} \omega_{lm}^* , \tag{29}$$

which employ essentially the same information as in the kinetic energy spectra, yet emphasize the small-wavelength features. These spectra are also shown in Fig. 8 (bottom frame) for both the standard and SEISMAR plate models. Both models show significant peaks in divergence at $l=2$, $l=4$ and 5, and $l=24$; however, only the peak $l=5$ is reflected in the vorticity spectra. Nevertheless, the vorticity spectra appears to track the divergence spectra but only for low degree, that is up to approximately $l=10$; for higher degree the spectra seem largely uncorrelated. This may reflect the influence of plate geometry at low degree on both spectra, while at higher degree we see that

GJI000 21/4/98 07:18:03 3B2 version 5.20
The Charlesworth Group, Huddersfield 01484 517077

the structure of divergent/convergent boundaries is largely independent of the structure of strike-slip boundaries. Finally, one can also see the power drop off for the SEISMAR model, indicating that the spherical harmonic series for the SEISMAR model is convergent; no such convergence is indicated for the standard model, as is to be expected for apparent singularities.

5 CONCLUSIONS

In this paper we have presented a continuous kinematic model of present-day plate motions allowing for (1) a realistic representation of plate shapes, and (2) incorporation of geophysical data on intraplate deformation in order to estimate plate-margin widths. A variety of data sets contain information about intraplate deformation, such as seismicity and stress distributions. To demonstrate how such data is used in the continuous plate model, we employ global seismicity to constrain plate-margin width. The mathematical treatment of how to (1) define analytically continuous plate shape functions, and (2) use geophysical data (seismicity in particular) to construct plate-margin width functions is presented in this paper; although the treatment as a whole is relatively convoluted, the individual steps are basic and straightforward. The resulting seismicity-based example, called the SEISMAR plate model, yields a detailed and quantifiable representation of the horizontal divergence and radial vorticity fields (which are precise measures of poloidal and toroidal motion). Employing finite margin widths allows these fields to be analytically calculable (as opposed to being singularities in the standard plate model) and permits the representation of diffuse margins. The kinetic energy spectra and partitioning of the SEISMAR model are not greatly different from the standard plate model, as expected and desired; most of the minor differences arise because, with finite margins (and thus non-infinite divergence and vorticity), a more accurate weighting can be given to the contribution of plate spin to the toroidal energy. Although the SEISMAR model represents one example of combining geophysical data with a continuous plate model, it provides the first effort to incorporate intraplate deformation data into a global plate-tectonic model and is therefore a significant adjustment to the theory of plate tectonics.

REFERENCES

Bercovici, D., 1993. A simple model of plate generation from mantle flow, *Geophys. J. Int.,* **114,** 635–650.

Bercovici, D., 1995a. A source-sink model of the generation of plate tectonics from non-Newtonian mantle flow, *J. geophys. Res.,* **100,** 2013–2030.

Bercovici, D., 1995b. On the purpose of toroidal flow in a convecting mantle, *Geophys. Res. Lett.,* **22,** 3107–3110.

Bercovici, D., 1996. Plate generation in a simple model of lithosphere-mantle flow with dynamic self-lubrication, *Earth planet. Sci. Lett.,* **144,** 41–51.

Bercovici, D., 1998. Generation of plate tectonics from lithosphere-mantle flow and void volatile self-lubrication, *Earth planet. Sci. Lett.,* **154,** 139–151.

Bercovici, D., & Wessel, P., 1994. A continuous kinematic model of plate-tectonic motions, *Geophys. J. Int.,* **119,** 595–610.

DeMets, C., Gordon, R.G., Argus, D.F. & Stein, S., 1990. Current plate motions, *Geophys J. Int.,* **101,** 425–478.

DeMets, C., Gordon, R.G., Argus, D.F., Stein, S., 1994. Effect of recent revisions to the geomagnetic reversal time scale on estimates of current plate motions, *Geophys. Res. Lett.,* **21,** 2191–2194.

Hager, B.H., & O'Connell, R.J., 1978. Subduction zone dip angles and flow driven by plate motion, *Tectonophysics,* **50,** 111–133.

Hager, B.H., & O'Connell, R.J., 1979. Kinematic models of large-scale flow in the Earth's mantle, *J. geophys. Res.,* **84,** 1031–1048.

Hager, B.H., & O'Connell, R.J., 1981. A simple global model of plate dynamics and mantle convection, *J. geophys. Res.,* **86,** 4843–4867.

O'Connell, R.J., Gable, C.W., & Hager, B.H., 1991. Toroidal-poloidal partitioning of lithospheric plate motion, in *Glacial Isostasy, Sea Level and Mantle Rheology,* pp. 535–551, eds Sabadini, R. & Lambeck, K., Kluwer Academic, Norwell, MA.

Pollitz, F.F., 1988. Episodic North American and Pacific plate motions, *Tectonics,* **7,** 711–726.

Rousseeuw, P.J. & Leroy, A.M., 1987. *Robust Regression and Outlier Detection,* Wiley, New York, NY.

Sandwell, D.T. & Smith, W.H.F., 1997. Marine gravity anomaly from Geosat and ERS-1 satellite altimetry, *J. geophys. Res.,* **102,** 10 039–10 054.

Smith, W.H.F. & Sandwell, D.T., 1994. Bathymetric prediction from dense satellite altimetry and sparse shipboard bathymetry, *J. geophys. Res.,* **99,** 21 903–21 824.

Weissel, J.K., 1980. Evidence for Eocene oceanic crust in the Celebes Basin, in *The Tectonic and Geologic Evolution of Southeast Asian Seas and Islands,* ed. Hayes, D.E., AGU, Washington, DC, *Geophys. Monogr.,* **23,** 37–47.

Wiens, D.A. *et al.*, 1985. A diffuse plate boundary model for Indian ocean tectonics, *Geophys. Res. Lett.,* **12,** 429–432.

Zhong, S. & Gurnis, M. 1995a. Mantle convection with plates and mobile, faulted plate margins, *Science,* **267,** 838–843.

Zhong, S. & Gurnis, M. 1995b. Towards a realistic simulation of plate margins in mantle convection, *Geophys. Res. Lett.,* **22,** 981–984.

Zhong, S. & Gurnis, M., 1996. Interaction of weak faults and non-Newtonian rheology produces plate tectonics in a 3D model of mantle flow, *Nature,* **267,** 838–843.

Zoback, M.L. & Burke, K., 1993. Lithospheric stress patterns: a global view, *EOS, Trans. Am. geophys. Un.,* **74,** 609–618.

GJI000 21/4/98 07:18:23 3B2 version 5.20
The Charlesworth Group, Huddersfield 01484 517077

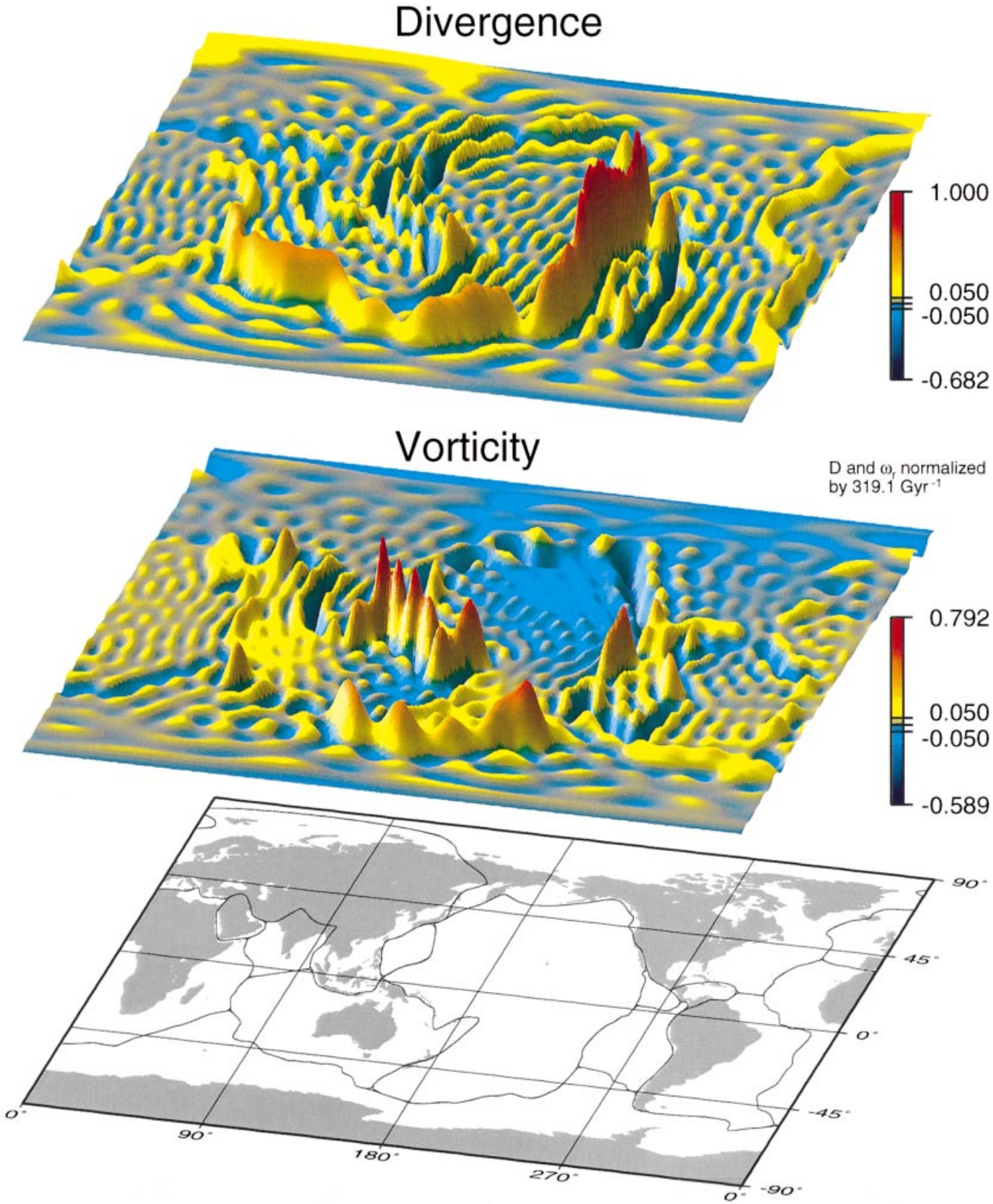

Figure 6. Surfaces of horizontal divergence and radial vorticity (with a world map at the bottom for orientation) for the Earth's present-day plate motions based on vector spherical harmonic transforms of the velocity field for the standard discontinuous plate-tectonic model (with zero margin widths).

GJI000 21/4/98 07:18:25 3B2 version 5.20
The Charlesworth Group, Huddersfield 01484 517077

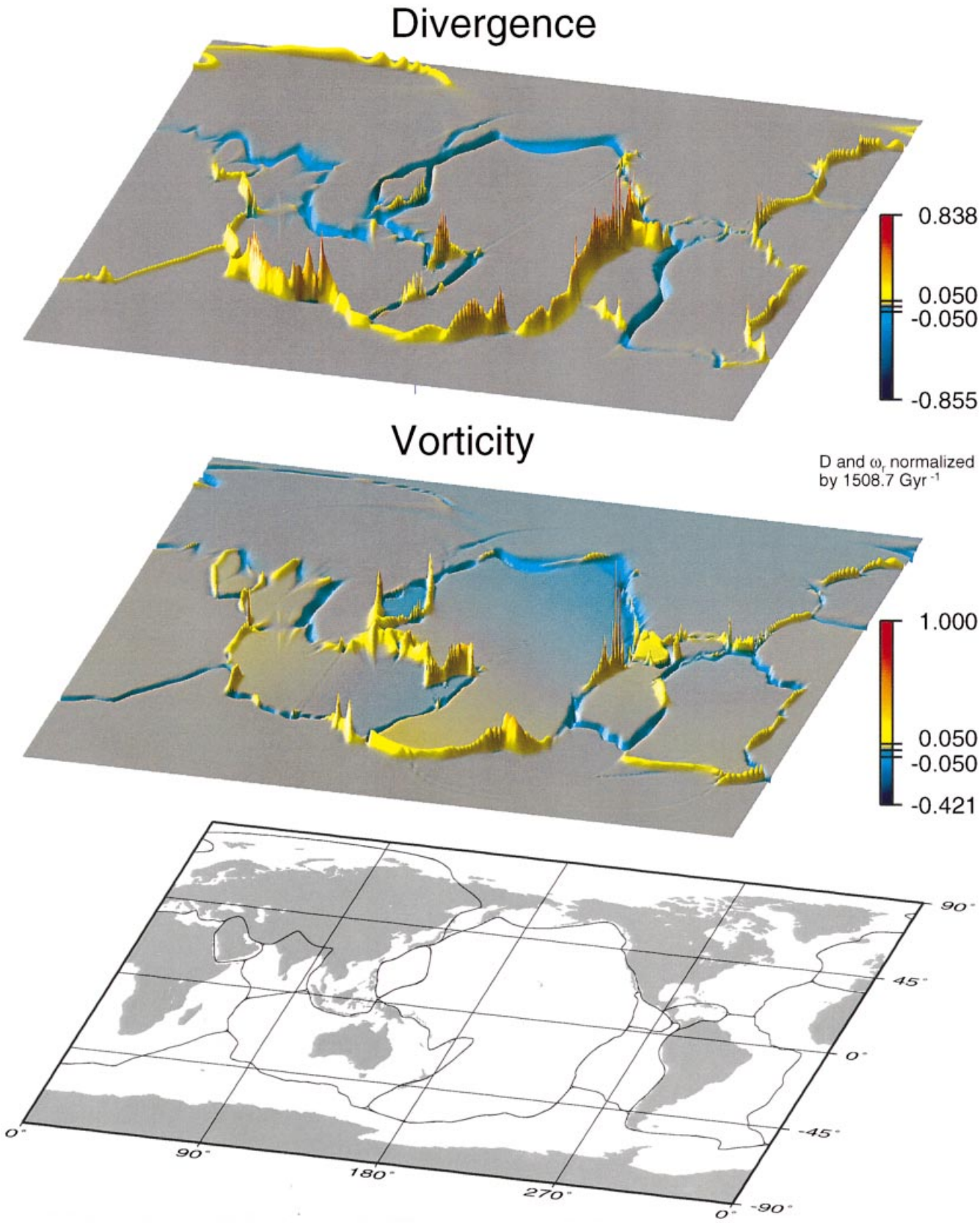

Figure 7. Same as Fig. 6 but with horizontal divergence and radial vorticity calculated directly from the velocity field of the SEISMAR plate model.

GJI000 21/4/98 07:18:27 3B2 version 5.20
The Charlesworth Group, Huddersfield 01484 517077